OPEN ACCESS Freely available online

PLOS ONE

Modeling Spatial Patterns of Soil Respiration in Maize Fields from Vegetation and Soil Property Factors with the Use of Remote Sensing and Geographical Information System

Ni Huang[1], Li Wang[1]*, Yiqiang Guo[2], Pengyu Hao[1], Zheng Niu[1]

1 The State Key Laboratory of Remote Sensing Science, Institute of Remote Sensing and Digital Earth, Chinese Academy of Sciences, Beijing, China, **2** Land Consolidation and Rehabilitation Center, Ministry of Land and Resources, Beijing, China

Abstract

To examine the method for estimating the spatial patterns of soil respiration (R_s) in agricultural ecosystems using remote sensing and geographical information system (GIS), R_s rates were measured at 53 sites during the peak growing season of maize in three counties in North China. Through Pearson's correlation analysis, leaf area index (LAI), canopy chlorophyll content, aboveground biomass, soil organic carbon (SOC) content, and soil total nitrogen content were selected as the factors that affected spatial variability in R_s during the peak growing season of maize. The use of a structural equation modeling approach revealed that only LAI and SOC content directly affected R_s. Meanwhile, other factors indirectly affected R_s through LAI and SOC content. When three greenness vegetation indices were extracted from an optical image of an environmental and disaster mitigation satellite in China, enhanced vegetation index (EVI) showed the best correlation with LAI and was thus used as a proxy for LAI to estimate R_s at the regional scale. The spatial distribution of SOC content was obtained by extrapolating the SOC content at the plot scale based on the kriging interpolation method in GIS. When data were pooled for 38 plots, a first-order exponential analysis indicated that approximately 73% of the spatial variability in R_s during the peak growing season of maize can be explained by EVI and SOC content. Further test analysis based on independent data from 15 plots showed that the simple exponential model had acceptable accuracy in estimating the spatial patterns of R_s in maize fields on the basis of remotely sensed EVI and GIS-interpolated SOC content, with R^2 of 0.69 and root-mean-square error of 0.51 μmol CO_2 m^{-2} s^{-1}. The conclusions from this study provide valuable information for estimates of R_s during the peak growing season of maize in three counties in North China.

Citation: Huang N, Wang L, Guo Y, Hao P, Niu Z (2014) Modeling Spatial Patterns of Soil Respiration in Maize Fields from Vegetation and Soil Property Factors with the Use of Remote Sensing and Geographical Information System. PLoS ONE 9(8): e105150. doi:10.1371/journal.pone.0105150

Editor: Ben Bond-Lamberty, DOE Pacific Northwest National Laboratory, United States of America

Received March 13, 2014; **Accepted** July 7, 2014; **Published** August 26, 2014

Data Availability: The authors confirm that all data underlying the findings are fully available without restriction. Data have been deposited to Dryad with the DOI: doi:10.5061/dryad.12528.

Funding: This work was supported by the National Natural Science Foundation of China (41301498), the Public Service Sectors (Ministry of Land and Resources) Special Fund Research (201311127), the Special Foundation for Young Scientists of the State Laboratory of Remote Sensing Science (13RC-07), and the Major State Basic Research Development Program of China (2013CB733405). The funders had no role in study design, data collection and analysis, decision to publish, or preparation of the manuscript.

Competing Interests: The authors have declared that no competing interests exist.

* Email: wangli@radi.ac.cn

Introduction

Soil CO_2 efflux from terrestrial ecosystems to the atmosphere has been considered the second largest global carbon flux and is a vital component of ecosystem respiration [1]. In recent decades, significant progress has been made in identifying the biophysical factors that influence soil respiration (R_s) to predict soil CO_2 emission accurately in time and space [2–4].

The majority of R_s arises from root and microbial tissue. Therefore, understanding the spatial and temporal changes of these sources will facilitate the modeling of R_s. However, the large spatial and temporal heterogeneity of root and microbial activity within the landscape and the covariation of potentially important factors (i.e., temperature and water content) pose great challenges to the development of mechanistically based models that account for spatial and temporal variability in R_s [2]. Thus, many different statistical models of R_s have been developed on the basis of data collected from different ecosystems [5]. Numerous studies have established R_s models based on soil temperature, soil moisture, or both [6,7]. Aside from soil temperature and moisture, plant productivity proxies [e.g., leaf area index (LAI), canopy chlorophyll content (Chl_{canopy}), and plant biomass] [8–10] and soil properties [e.g., soil organic carbon (SOC) content, soil total nitrogen (STN) content, and soil C and N ratio (soil C/N)] [11,12] also potentially influence R_s and are often included in models of R_s. However, most of the factors that affect variations in R_s tend to be derived through field measurements [13]. Furthermore, direct observation of these variables across long time spans or large spatial scales is expensive because of the required manpower and material resources. A simple method to derive data related to variations in R_s is necessary to facilitate the determination of the spatial and temporal distribution of R_s.

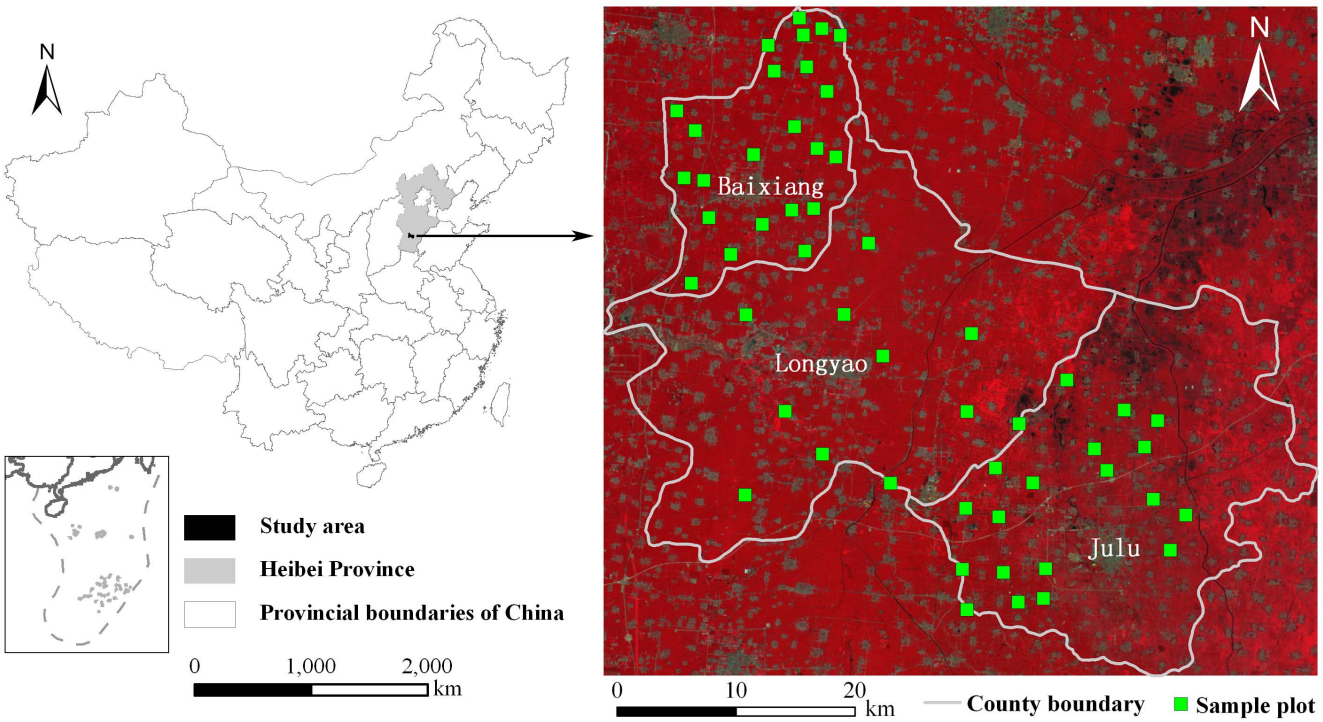

Figure 1. Spatial location of the sample plots for field experiments in three counties in North China. The box in the bottom left corner of Figure 1 shows the South China Sea islands.
doi:10.1371/journal.pone.0105150.g001

Remote sensing and geographical information system (GIS) provide powerful tools for data acquisition, spatial analysis, and graphical display [14–16]. In the field of global change research, significant advances have been made in the development and application of remote sensing and GIS. These advances include land cover and land-use changes [17,18], environmental vulnerability and risk assessment [19,20], ecological restoration and management [21–23], and terrestrial ecosystem carbon cycle [24–26]. However, applying the data derived from remote sensing and GIS into R_s modeling remains controversial, especially for remote sensing data, because remotely sensed data in principle are independent measurements of site properties, not functionally important variables (e.g., soil temperature, soil moisture, and plant growth variables) that control R_s [3,27,28]. On the basis of statistical analysis of field experiments, previous studies found that remotely sensed vegetation indices (VIs) correlate with R_s in crop sites that lack drought stress [10] and can be used to model the spatial patterns of R_s during the peak growing season of alpine grasslands in the Tibetan Plateau [26]. However, few studies explore the potential of remote sensing and GIS data for estimating the spatial patterns of R_s in agricultural land, which may be affected by more complex factors than natural grasslands because of the influence of human activity. Although modern agriculture has successfully increased food production, the processes involved have profoundly affected the global carbon cycle through tillage, drainage and conversion of natural to agricultural ecosystems [29,30]. Therefore, a simple method should be identified to study the spatial characteristics of R_s in agricultural ecosystems.

This study aims to examine a potential new approach for estimating the spatial patterns of R_s during the peak growing season of maize by using remote sensing and GIS technology in Baixiang, Longyao and Julu Counties, which are typical agricultural areas in the north plain of China. Studying the spatial characteristics of soil CO_2 efflux in maize fields will contribute to eco-agricultural development.

Materials and Methods

Ethics Statement

No specific permissions were required for the 53 sample plots in this study. We confirmed that the field studies did not involve endangered or protected species, and the specific location of the sample plots was provided in the manuscript (Fig. 1).

Study Site

The study site is situated within three counties (Baixiang, Longyao and Julu) in Southern Hebei Province of North China (Fig. 1). The total area of the study site is 1.64×10^3 km^2. This area is located in the North China Plain with a flat open terrain, single landform type, and a mean elevation of 30 m above sea level. Calcareous alluvial soil with high capacity to retain water and fertilizer is the main soil type in the study area. The study site is suitable for farming, and maize is the main crop. The climate is continental monsoon with four distinct seasons and adequate light and heat resources. Long records of meteorological data near the study site (http://cdc.cma.gov.cn) indicate that the mean annual temperature is 13.5°C with the coldest temperatures in January and the hottest in July. The mean annual precipitation is 502.8 mm, but precipitation is distributed unevenly in the four seasons with the greatest precipitation occurring in summer (362.5 mm). Therefore, drought influences agricultural development, and agriculture mainly involves irrigation in this study site.

Fifty-three sample plots located in the maize fields were identified within the study site (Fig. 1). The distance between any two sample plots was larger than 2 km. Each sample plot

(greater than 100 m×100 m) has a large maize area, flat terrain, and maize under uniform growing conditions. All measurements were performed from August 11, 2013 to August 20, 2013, which corresponded to the tassel stage and peak growing period of maize. During the 10 days of field measurements, continuous measurements were performed, except on August 12 because of a minor precipitation event. Therefore, all field measurements required 9 days.

Field measurements

Soil respiration measurements. In each sample plot, R_s was measured by using a soil respiration chamber (LI-6400-09; LiCor, Lincoln, Nebraska, USA) connected to a portable photosynthesis system (LI-6400; LiCor, Lincoln, Nebraska, USA). The soil respiration chamber was mounted on a PVC soil collar that was sharpened at the bottom. Each PVC collar (5 cm long, 11 cm inside diameter) was inserted 2 cm to 3 cm into the ground and was installed at least 24 h prior to performing any measurements. To reduce the difference in root biomass, soil collars were placed in three locations on the basis of their distance to the maize plant: near a maize plant, inter-plant, and inter-row. Two collars were placed in each of the three positions for each R_s measurement. At least three to four consecutive measurements on each collar were performed to prevent any systematic error in the R_s estimates. An average R_s value was used for each collar, and the average value from six collars was used to represent the R_s value at plot level. Each R_s measurement was conducted between 09:00 h and 15:00 h (local time) because fluxes measured during this time interval are usually representative of the daily mean flux.

Soil temperature and soil moisture measurements. After the soil respiration measurement on a PVC soil collar in each plot, soil temperature and soil moisture were measured in this collar to minimize sample difference. Soil temperature was measured at a 10 cm depth (T_{s10}) by using a ground thermometer. Volumetric soil moisture at a depth of 0 cm to 20 cm (SM_{20}) was determined by using a portable time domain reflectometry probe (HydroSense, Campbell, USA). Thus, six soil temperature and moisture measurements were performed in each plot. The average value was used to represent soil temperature or soil moisture at the plot level.

Maize biophysical parameter measurements. LAI was measured by using an LAI-2000 (LI-COR Inc., Lincoln, Nebraska). In each plot, six representative positions were selected for LAI measurement, and in every position, two repeated measurements were performed. Leaf chlorophyll content (Chl_{leaf}) was determined by using a portable chlorophyll meter (SPAD-502, New Jersey, USA). Fully expanded leaves, which depended on the height of the maize plant, were randomly selected from three locations that corresponded to the upper, middle, and lower parts of the maize plant. For each leaf location, 10 SPAD values were randomly collected. The vertical leaf area distribution in maize canopy was analyzed by measuring the area of each green leaf from the bottom to the top of eight randomly distributed maize plants with the use of an area meter (LI-3100, LI-COR, Lincoln, Nebraska). The area-weighted mean SPAD reading was used to derive Chl_{leaf}. However, the SPAD reading was in arbitrary units rather than in actual amounts of chlorophyll per unit area of the leaf tissue. A transform relationship exists between the SPAD readings and the actual chlorophyll content in maize [31]. To convert the SPAD readings to chlorophyll content per unit leaf area ($\mu g\ cm^{-2}$), this study used the transform relationship ($Chl_{leaf} = 0.95 \times SPAD\ reading - 3.25$) derived by Wu et al. [32] in maize plots, and the same SPAD meter was employed in this study. Chl_{canopy} was then determined by using the following equation:

$$Chl_{canopy} = Chl_{leaf} \times GLAI \quad (1)$$

where Chl_{canopy} is the canopy chlorophyll content ($g\ m^{-2}$), Chl_{leaf} is the leaf chlorophyll content of maize ($g\ m^{-2}$), and GLAI represents the green leaf area per unit ground area.

In each sample plot, three representative maize plants were harvested for aboveground biomass (AGB) measurement. These fresh maize plants were sealed in a plastic bag and immediately transported to a nearby laboratory for subsequent analysis. Thereafter, fresh samples were oven dried at 65°C until the mass of the sample reached a constant weight. The AGB in each plot can be derived by multiplying the average dry weight per plant ($g\ plant^{-1}$) and the average plant density of maize ($plants\ m^{-2}$).

Soil property measurements. Soil within the six PVC collars in each plot was destructively sampled after measuring R_s, soil temperature and soil moisture. Soil was sampled to a depth of approximately 20 cm by a cylindrical soil driller (4 cm diameter, 20 cm height), in which fine root biomass and microbial activity are the highest [33,34]. These collected soil samples were sealed in plastic bags and stored at room temperature while being transported to the laboratory. Six collected soil samples in each plot were uniformly mixed to form a composite sample for laboratory analysis. The composite sample was air-dried in the laboratory to a constant weight for soil chemical analyses. The air-dried soil samples were ground to pass through a 0.2 mm sieve after any visible plant tissues and debris were manually removed. The SOC content was estimated by using the standard Mebius method [35]. The STN content was analyzed by using the Kjeldahl digestion procedure [36]. In this study, soil C/N was calculated by the ratio of SOC and STN contents.

Table 1. Calculation for vegetation indices [a].

Vegetation index	Formula	Reference
Normalized difference vegetation index	$NDVI = \frac{R_{Nir} - R_{Red}}{R_{Nir} + R_{Red}}$	Rouse et al. [47], Gamon et al. [48]
Modified soil adjusted vegetation index	$MSAVI = \frac{2R_{Nir} + 1 - \sqrt{(2R_{Nir}+1)^2 - 8(R_{Nir} - R_{Red})}}{2}$	Qi et al. [49]
Enhanced vegetation index	$EVI = 2.5 \times \frac{R_{Nir} - R_{Red}}{1 + R_{Nir} + 6 \times R_{Red} - 7.5 \times R_{Blue}}$	Huete et al. [50]

[a] R_{Blue}, R_{Red}, and R_{Nir} are reflectance of blue, red, and NIR band in the HJ-1A CCD optical image, respectively.

doi:10.1371/journal.pone.0105150.t001

Table 2. Pearson's correlation among soil respiration and factors affecting soil respiration in maize fields during the peak growing season in three counties in North China.

	R_s	T_{s10}	SWC_{20}	Chl_{canopy}	LAI	AGB	SOC content	STN content	Soil C/N
R_s	1.00	−0.27	−0.18	0.54***	0.75***	0.59***	0.76***	0.59***	−0.23
T_{s10}		1.00	0.18	−0.15	−0.28	−0.27	−0.49**	−0.66***	0.51**
SWC_{20}			1.00	−0.17	−0.05	−0.07	0.16	−0.00	0.06
Chl_{canopy}				1.00	0.83***	0.81***	0.26	0.20	−0.18
LAI					1.00	0.76***	0.44**	0.38*	−0.28
AGB						1.00	0.45**	0.34*	−0.15
SOC content							1.00	0.78***	−0.29
STN content								1.00	−0.79***
Soil C/N									1.00

R_s is the daily mean soil respiration rate (μmol CO_2 m^{-2} s^{-1}), T_{s10} is the soil temperature at 10 cm depth (°C), SWC_{20} is the soil water content at 0 cm to 20 cm depth (m^3 m^{-3}), Chl_{canopy} is the canopy chlorophyll content (g m^{-2}), LAI is the leaf area index, AGB is the aboveground biomass (kg m^{-2}), SOC content is the soil organic carbon content (g kg^{-1}), STN content is the soil total nitrogen content (g kg^{-1}), and soil C/N is the soil C: N ratio. Significance levels:
*$p<0.05$,
**$p<0.01$,
***$p<0.001$.
doi:10.1371/journal.pone.0105150.t002

Spatial data acquisition

Maize classification data. This study aimed to derive the spatial distribution of R_s in maize fields based on the field measurements at the plot scale. Maize classification data is necessary to spatially extrapolate R_s at the plot scale to the whole study area. Multi-temporal normalized difference vegetation index (NDVI) data collected over the growing season were used to classify maize at the study site [37–39]. Clouds are common occurrences in the study area during the growing season. Thus, obtaining a time sequence of cloud-free scenes is difficult. Two types of satellite data were used to establish the time-series NDVI data. One was the Operational Land Imager (OLI) image of Landsat 8, and the other was the small constellation for environmental and disaster mitigation (HJ-1A and B) charge coupled device (CCD) image [40–42]. Five scenes of OLI images acquired on May 3, 2013, May 19, 2013, July 6, 2013, October 10, 2013, and October 26, 2013 were downloaded from the U.S. Geological Survey (http://earthexplorer.usgs.gov/). Three HJ-1A and B CCD optical images acquired on June 6, 2013, August 17, 2013, and September 15, 2013 were downloaded from the China Center for Resource Satellite Data and Applications (http://www.cresda.com). The two types of remote sensing images exhibit same spatial resolution (30 m). The 30 m spatial resolution is appropriate for classifying maize patterns in the study area given the relatively large field in the region, which could spatially corresponded to five or more 30 m pixels. The strong relationship of the NDVI with biophysical vegetation characteristics, such as LAI and green biomass [43,44], enables the discrimination of land cover types on the basis of their unique phenological responses. Before land-use classification, pre-processing (i.e., radiometric calibration, atmospheric correction and geometric correction) of OLI images and HJ-1A and B CCD optical images was accomplished by using the Environment for Visualizing Images (ENVI) software (Version 4.7, Research Systems Inc., Boulder, Colorado, USA) [45,46]. This process ensured the consistency between the two types of remote sensing data and the seasonality of the NDVI time series. The maximum likelihood classification method, integrated in the ENVI software, was applied to the eight-date NDVI time series that spanned one maize growing season of the study site.

Spectral vegetation index for vegetation biophysical parameter estimation. Three greenness indices, namely, NDVI, enhanced vegetation index (EVI), and modified soil adjusted vegetation index (MSAVI), were derived from the HJ-1A CCD optical image acquired on August 17, 2013 (Table 1) for vegetation biophysical parameter estimation. Previous studies reported that greenness VIs offer important and convenient measures for vegetation biophysical parameters, such as LAI and Chl_{canopy} [51–54]. Meanwhile, LAI and Chl_{canopy} are also found to be good indicators of plant canopy photosynthesis [55–57] and are used in the modeling of R_s [58]. To obtain the spatial patterns of vegetation biophysical parameters in maize fields, the spatial distribution of vegetation biophysical parameters over the whole study area was overlapped with the maize classification data.

Quantifying the spatial pattern of SOC content. Statistics and geostatistics have been widely applied to quantify the spatial distribution patterns of SOC at a regional scale [59–61]. Based on the theory of regionalized variables, geostatistics provides advanced tools to quantify the spatial features of soil parameters and to conduct spatial interpolation [62,63]. In this study, geostatistical analyses were performed by using the geostatistical analyst module of ArcGIS software (Version 9.3, 2008) to quantify the spatial pattern of SOC content. To obtain the spatial pattern of the SOC content in the maize fields, the spatial distribution of

Table 3. Spatial characteristics of soil respiration (R_s, μmol CO_2 m^{-2} s^{-1}), soil temperature at 10 cm depth (T_{s10}, °C), soil water content at 0 cm to 20 cm depth (SWC_{20}, m^3 m^{-3}), canopy chlorophyll content (Chl_{canopy}, g m^{-2}), leaf area index (LAI), aboveground biomass (AGB, kg m^{-2}), soil organic carbon content (SOC content, g kg^{-1}), soil total nitrogen content (STN content, g kg^{-1}) and soil C: N ratio (soil C/N) in maize fields during the peak growing season in three counties in North China.

Variables	Mean	Maximum	Minimum	CV (%)
R_s	5.43	7.33	2.64	15.45
T_{s10}	28.32	30.93	25.78	4.73
SWC_{20}	27.54	33.27	19.54	12.48
Chl_{canopy}	0.18	0.21	0.16	6.54
LAI	3.75	4.53	2.81	8.64
AGB	0.94	1.89	0.44	31.93
SOC content	11.86	17.26	6.40	16.71
STN content	1.25	1.78	0.53	24.47
Soil C/N	9.82	14.38	7.07	18.53

doi:10.1371/journal.pone.0105150.t003

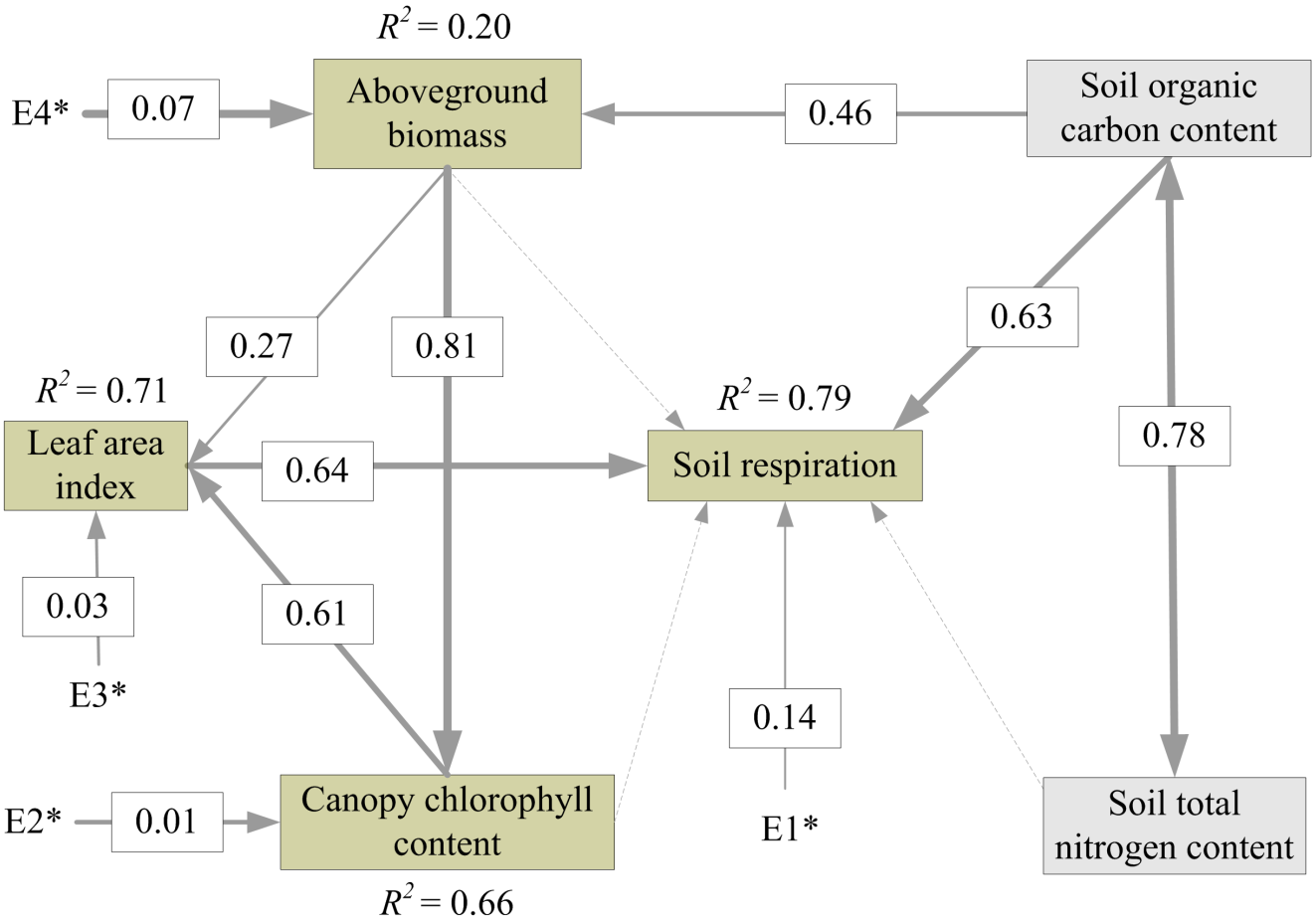

Figure 2. Final structural equation modeling (SEM) for soil respiration. Non-significant paths are shown in dashed line. The thickness of the solid arrows reflects the magnitude of the standardized SEM coefficients. Standardized coefficients are listed on each significant path. * represents error terms for observed variables, among them, E1, E2, E3, and E4 represent measurement errors for soil respiration, canopy chlorophyll content, leaf area index, and aboveground biomass, respectively.
doi:10.1371/journal.pone.0105150.g002

Table 4. Total, direct, and indirect effects in the structural equation modeling.

Variable	Direct effect	Indirect effect	Total
Soil respiration			
Aboveground biomass	−0.10*ns*	0.46	0.36
Soil organic carbon content	0.63	0.16	0.79
Soil total nitrogen content	−0.09*ns*	0.30	0. 21
Leaf area index	0.64	-	0.64
Canopy chlorophyll content	−0.04*ns*	0.39	0.35
Aboveground biomass			
Soil organic carbon content	0.46	-	0.46
Soil total nitrogen content	−0.01*ns*	-	−0.01*ns*
Leaf area index			
Aboveground biomass	0.27	0.50	0.77
Soil organic carbon content	-	0.35	0.35
Soil total nitrogen content	-	−0.01*ns*	−0.01*ns*
Canopy chlorophyll content	0.61	-	0.61
Canopy chlorophyll content			
Aboveground biomass	0.81	-	0.81
Soil organic carbon content	-	0.37	0.37
Soil total nitrogen content	-	−0.01*ns*	−0.01*ns*

These effects were calculated using standardized path coefficients. Non-significant effects are indicated by "*ns*".
doi:10.1371/journal.pone.0105150.t004

the SOC content over the whole study area was overlapped with the maize classification data.

Modeling spatial patterns of soil respiration

Identifying factors affecting spatial variability of soil respiration. The variables that explain the spatial variability of R_s are as follows: (1) soil properties, measured by SOC content, STN content and soil C/N; (2) environmental factors, encompassing T_{s10} and SM_{20}, and (3) plant photosynthesis proxy factors, including AGB, LAI and Chl_{canopy}. Pearson's correlation requires variables to be normally distributed and mutually independent. Each variable was tested for normal distribution by using the Shapiro–Wilk normality test and for randomness by the runs test of the Statistical Package for the Social Sciences (SPSS, Chicago, Illinois, USA). The results of the statistical analysis showed that each of these measured variables followed a normal distribution (Shapiro-Wilk, $p>0.05$) and showed randomness (runs test, $p>0.05$). Thus, Pearson's correlation analysis, as implemented in the SPSS software, was used to screen important variables that influence R_s. Five variables with statistically significant correlation ($p<0.05$) with R_s, namely, SOC content, STN content, LAI, AGB, and Chl_{canopy}, were screened out (Table 2). However, these variables were cross-correlated [64–66] and included both direct and indirect effects. To solve this problem, structural equation modeling (SEM) was used to evaluate explicitly the causal relationships among these interacting variables [67–69] and to divide the total effects of variables on R_s into direct and indirect effects. On the basis of the theoretical knowledge on the major factors that influence spatial patterns of R_s at regional scales [8,13,26], we developed an SEM model to relate R_s to SOC content, STN content, LAI, AGB, and Chl_{canopy}. This SEM model was used to identify the direct effect factors for R_s estimation. The SEM model was fitted by using AMOS 18.0 for Windows [70]. After using the SEM, the fit indices, namely, comparative fit index = 0.984 and goodness-of-fit index = 0.946. Thus, the theoretical model showed a good fit with the sample data.

Quantifying the spatial patterns of soil respiration in maize fields. In this study, the direct effect factors of R_s identified by SEM were used to estimate R_s. The spatial distribution data of these direct effect factors were first obtained on the basis of remote sensing or GIS to quantify the spatial patterns of R_s in maize fields. A simple exponential model that used the proxy data was then employed to estimate the spatial pattern of R_s during the peak growing season of maize. The accuracy of this method was examined by separating the observed data into two datasets through a random generator. One dataset consisted of 38 sample plots for analysis, whereas the other consisted of 15 for testing the accuracy of the R_s estimation.

Result

Spatial characteristics of soil respiration

Based on field-measured data at 38 plots, the daily mean R_s of maize during the peak growing season was 5.43 μmol CO_2 m^{-2} s^{-1} with a range of 2.64 μmol CO_2 m^{-2} s^{-1} to 7.33 μmol CO_2 m^{-2} s^{-1} and a coefficient of variation (CV) of 15.45% (Table 3). The spatial variability of soil temperature at 10 cm depth (T_{s10}) was relatively small at the study site with a CV of 4.73% and was far less than the spatial variation in soil water content at 0 cm to 20 cm depth (SWC_{20}). The AGB of maize showed greater spatial variability (CV = 31.93%) than LAI (CV = 8.64%) and Chl_{canopy} (CV = 6.54%).

Mean SOC content, STN content, and soil C/N at 0 cm to 20 cm depth in maize fields of the study site were 11.86 g kg^{-1} (ranged from 6.40 g kg^{-1} to 17.26 g kg^{-1}), 1.25 g kg^{-1} (ranged from 0.53 g kg^{-1} to 1.78 g kg^{-1}), and 9.82 (ranged from 7.07 to 14.38), respectively. Their CVs were not similar with the STN content which showed greater spatial variability than the SOC content and soil C/N.

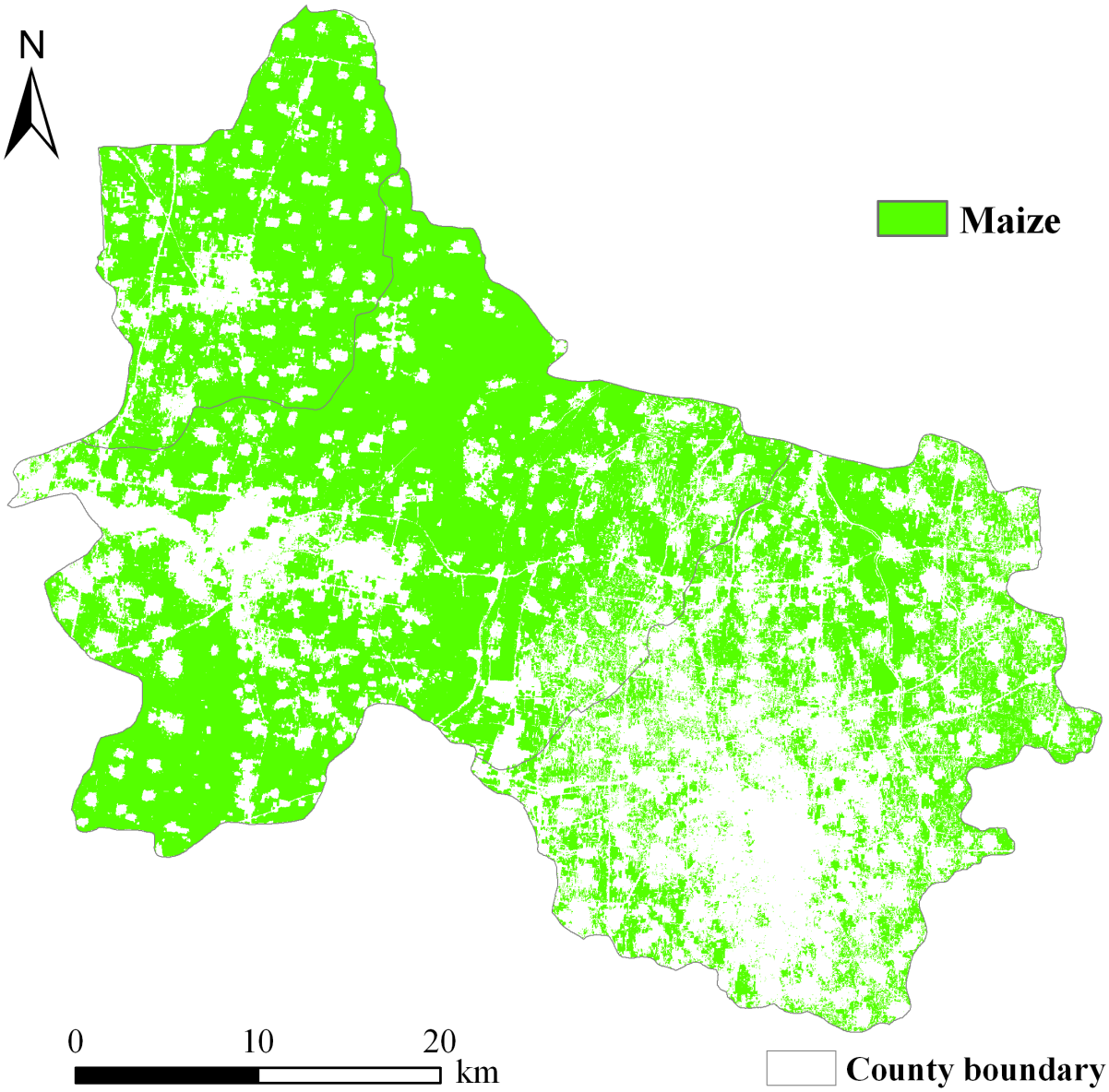

Figure 3. Maize classification map in three counties in North China.
doi:10.1371/journal.pone.0105150.g003

Factors driving spatial variability of soil respiration

Based on Pearson's correlation analysis, five variables with significant correlation with R_s, namely, Chl_{canopy}, LAI, AGB, SOC content, and STN content, were selected (Table 2). However, the five selected variables were intercorrelated (Table 2), and their relationships with R_s combined both direct and indirect correlations. Thus, an SEM model was further used to evaluate the causal relationships among these interacting variables. The final SEM explained 79% of the variation in R_s (Fig. 2). The direct, indirect, and total effects of the variables are shown in Table 4. Among the five selected variables, LAI and SOC content directly affected R_s and can be used to predict R_s with relatively high accuracy ($R^2 = 0.79$). The other three variables (i.e., Chl_{canopy}, ABG, and STN content), despite having a significant correlation with R_s, only affected R_s indirectly through their direct relationship with SOC content and LAI. Thus, the two direct effect factors were used to estimate R_s, and the spatially distributed data proxies of these two factors were used to quantify the spatial patterns of R_s in maize fields during the peak growing season.

Spatial data used for soil respiration estimation

Maize classification. The maize classification map of the study area is shown in Figure 3. The classification accuracy for maize at the study site could not be quantitatively assessed because of the limitation of the sample data. However, 53 sample plots were all located in the maize classification map, and the county-level maize patterns classified in the map were consistent with the general maize patterns across the three counties. In addition, the classified maize area was close to the maize area reported by the China County Statistical Yearbook [71]. Thus, the classification accuracy of maize was believed to be reasonable, and the maize classification map was then used to predict the spatial pattern of R_s during the peak growing season of maize.

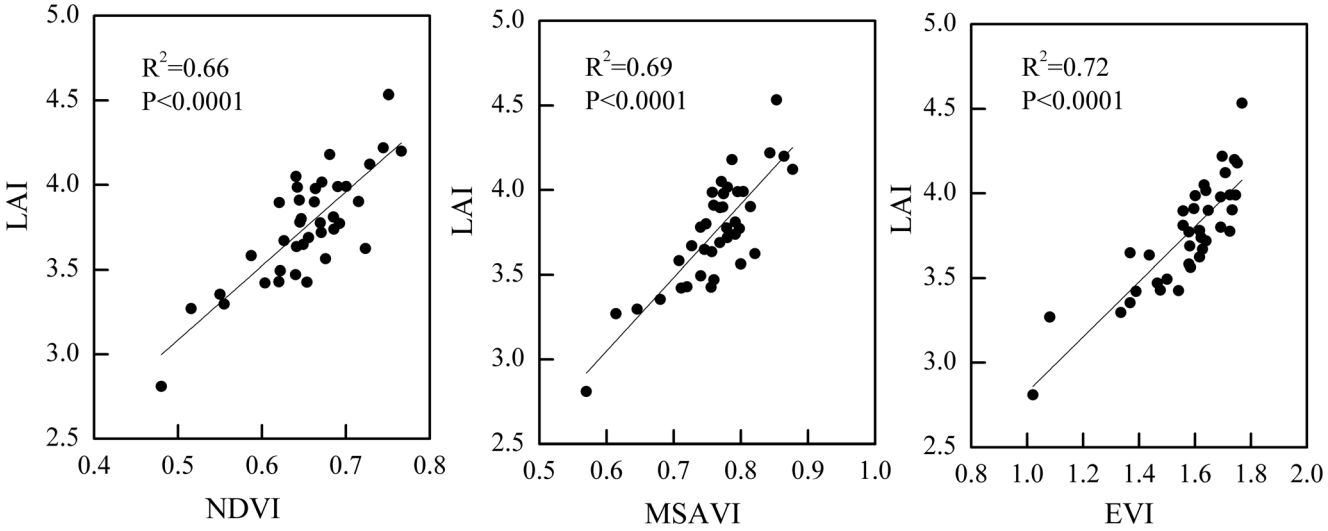

Figure 4. Linear relationships between three vegetation indices (VIs) and leaf area index (LAI) during the peak growing season of maize in three counties in North China (n = 38). The VIs are: normalized difference vegetation index (NDVI), enhanced vegetation index (EVI), and modified soil adjusted vegetation index (MSAVI).
doi:10.1371/journal.pone.0105150.g004

LAI estimation from spectral vegetation index. Among the three greenness indices calculated from the optical image of HJ-1A satellite, EVI showed the best linear relationship with LAI, with a determination coefficient (R^2) of 0.72, followed by MSAVI and NDVI (Fig. 4). The explanation of LAI variance increased from 66% to 72% when EVI was used instead of NDVI for LAI estimation, and this increase was statistically significant ($p<0.05$). However, EVI and MSAVI did not exhibit a significant difference in explaining the variation in LAI, despite EVI having a slightly better relationship with LAI than MSAVI. Thus, EVI was used as a proxy for LAI to estimate R_s during the peak growing season of maize for simplicity. The spatially distributed EVI during the peak growing season of maize exhibited relatively small variability (Fig. 5). Overall, the EVI in the north and southwest parts of the study site (i.e., Baixiang and Longyao Counties) showed a high value. Relatively low EVI values mainly occurred in the southeast parts of the study site (i.e., Julu County), especially the northwest Julu County (Fig. 5).

Spatial distribution of SOC content. Kriging interpolation was performed by using ArcGIS 9.3 software to produce the spatial distribution map of the SOC content in maize fields of the study area. A cell size of 30 m×30 m was selected for the spatial interpolation to match the spatial resolution of images from OLI and HJ-1A/B. The final result of this spatial interpolation process is shown in Figure 6. Based on the spatial distribution map of the SOC content in maize fields, SOC content values were higher in the northwest and southwest parts of the study area than in the southeastern part.

Spatial distribution of soil respiration

The EVI and SOC content were used to estimate the spatial pattern of R_s during the peak growing season of maize on the basis of a simple exponential model. The geo-location information (latitude and longitude) of the 38 sample plots was used in the extraction of pixels. Pixels that contained these plots from the spatial distribution maps of EVI and SOC content data (Figs. 5 and 6) were extracted. These data were used to determine the model parameters by least-squares fitting. The resulting model was as follows:

$$R_s = 1.57 \times \exp(0.44 \times \mathrm{EVI} + 0.05 \times \mathrm{SOC\ content}) \quad (2)$$

$$(n = 38,\ R^2 = 0.73)$$

where R_s refers to the daily mean soil respiration rate in μmol CO_2 m^{-2} s^{-1}; EVI refers to enhanced vegetation index, as a proxy for LAI; and SOC content is the soil organic carbon content (g kg^{-1}) in maize fields of the study area. Eq. (2) was employed to predict the spatial pattern of R_s from spatially distributed EVI and SOC content data during the peak growing season of maize (Figs. 5 and 6). The spatial variation in R_s showed a pattern similar to that in SOC content (Figs. 6 and 7).

Figure 8 shows the accuracy assessment result of the R_s prediction model. The field measured R_s was comparable with the spatial data predicted R_s. Based on the independent test dataset, EVI and SOC content accounted for 69% of the spatial variation in ground-measured R_s, and the RMSE was 0.51 μmol CO_2 m^{-2} s^{-1}. The result of the accuracy assessment suggests that the prediction model, which used EVI and SOC content as the dependent variables, was effective in estimating R_s in maize fields during the peak growing season.

Discussion

Relationships between LAI and three VIs

In this study, in situ measured data were obtained during the peak growing period of maize (corresponding to the tassel stage of maize). The effect of soil background on the spectral reflectance of remote sensing images was negligible during this period because the maize cover was higher with LAI ranging from 2.81 to 4.53. The difference in the capability of spectral vegetation index (VI) responding to LAI variation mainly depended on the sensitivity of VI to the canopy structural variation of maize. Thus, the VI modified the effect of soil reflectance (i.e. MSAVI) did not exhibit a significantly greater advantage than NDVI, which is strongly affected by soil reflectance in sparsely vegetated areas [50]. EVI, which is more sensitive to variation in dense vegetation than

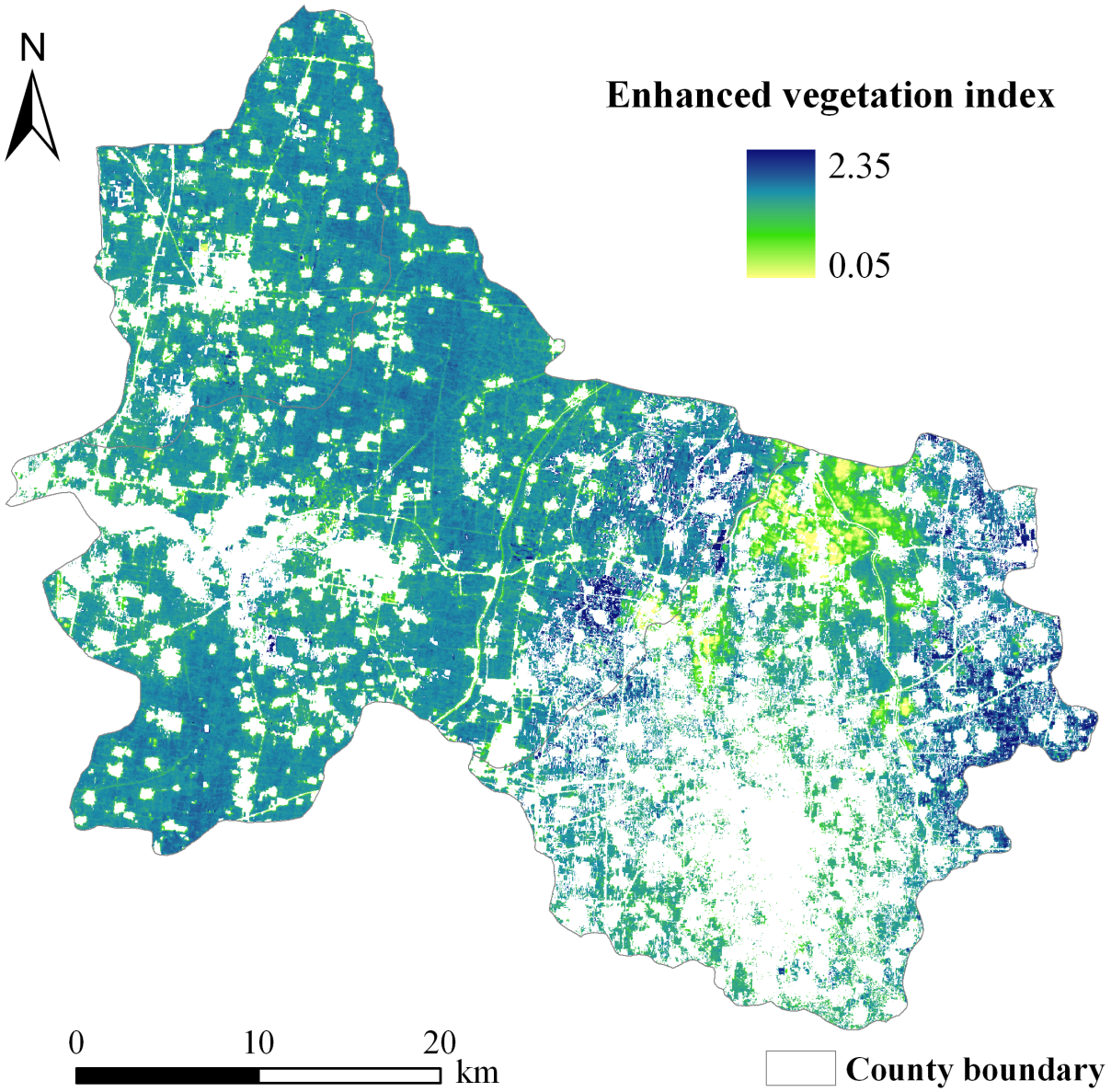

Figure 5. Spatial distribution map of enhanced vegetation index in maize fields in three counties in North China.
doi:10.1371/journal.pone.0105150.g005

NDVI [50], showed the best relationship with the LAI of maize. This result was consistent with our previous study [58] that was conducted in irrigated and rainfed maize fields located at the University of Nebraska, Agricultural and Research Development Center, Mead, Eastern Nebraska, USA.

Measurement accuracy of SOC content

Field measurement data revealed that the SOC content at 0 cm to 20 cm depth in the maize fields ranged from 6.4 g kg^{-1} to 17.3 g kg^{-1}, and the mean value was 12.01 g kg^{-1}. For the mean dry land SOC content in North China, the value appeared to be higher than the previous estimate (0.83 from the average of 268 sample points) [72]. This difference was partly attributed to the fact that only the SOC content in maize fields, not in all dry land types, was considered. Most maize fields in the study site were on a winter wheat/maize rotation, and wheat straw was returned to the soil. The high productivity of maize crops contributed to the development of a thick A horizon and high SOC content [73,74]. Additionally, only the SOC content in maize fields at 0 cm to 20 cm depth was analyzed, whereas previous studies estimated the SOC content on the basis of organic carbon content to a depth of 1 m [72,75,76]. In agricultural land, soil depth at 0 cm to 20 cm is located in the cultivation layer and has a higher SOC content than the SOC content at the deeper soil layers [34]. This condition contributed to the higher SOC content from the measured soil property data than the previous estimate.

Factors affecting spatial pattern of soil respiration

The spatial differences in R_s at the study site can be mainly attributed to the differences in vegetation productivity and soil property factors among the sample plots, whereas soil temperature and soil moisture served a minor function in regulating the spatial pattern of R_s. A previous study also demonstrated that site variables that reflect site productivity (e.g., LAI or aboveground

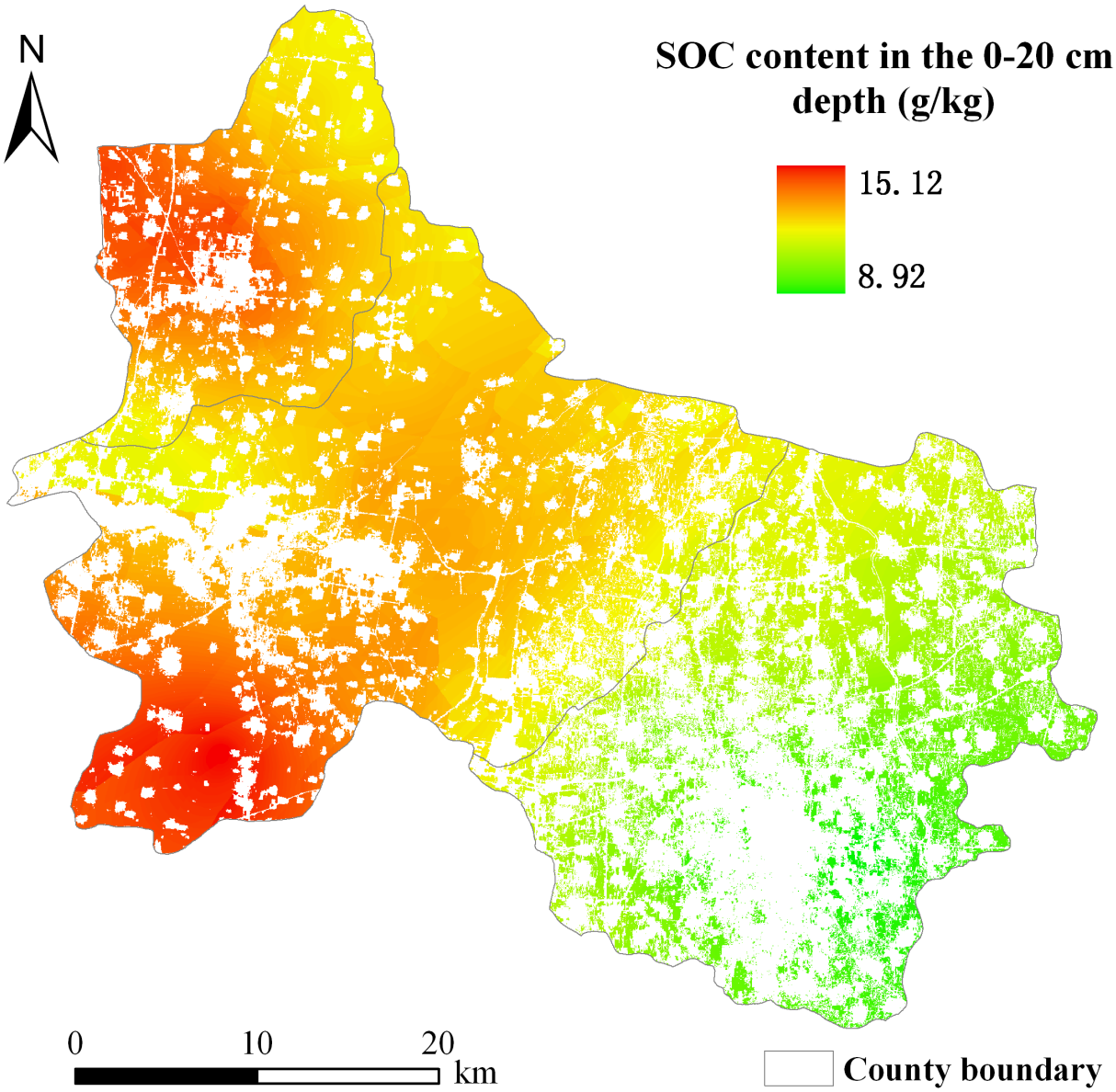

Figure 6. Spatial distribution map of soil organic carbon (SOC) content in the 0–20 cm depth in maize fields in three counties in North China.
doi:10.1371/journal.pone.0105150.g006

net primary productivity) will provide a useful approach for large-scale estimates of regional R_s in terrestrial ecosystems [8]. Soil temperature evidently serves a predominant function in the spatial variations of R_s across sites of climatically contrasting environments [4]. However, at a local scale or under similar climatic conditions, other biological and biophysical factors, such as vegetation productivity and the size of organic carbon pools, may prevail as dominant drivers of R_s [4,77]. At a local scale, the spatial variation in T_{s10} in the study site was small (CV = 4.73%). Thus, soil temperature did not affect the spatial pattern of R_s. Although soil moisture in the maize fields showed a relatively large spatial variation (CV = 12.48%), this variation did not reach a degree that will affect the spatial dynamics of R_s. The soil C quantity and substrate quality factors (i.e., SOC and STN contents) were consistently and strongly correlated with one another and significantly affected the variation in R_s [5,12,13]. However, SEM results showed that the STN content only affected R_s indirectly through the direct effect on the SOC content at the study site.

During the peak growing season of maize, biophysical parameters, such as LAI, Chl_{canopy}, and AGB, were important variables that determined the size of the photosynthetic capacity [56,78]. However, these variables are not truly independent, and a correlation between one of them and R_s may lead to a correlation of the other with R_s. In this study, R_s was strongly correlated with LAI, Chl_{canopy} and AGB of maize fields, whereas LAI was the only variable directly related to R_s during the peak growing season of maize on the basis of SEM analysis.

The direct effect factors of R_s were used to estimate the spatial variability of R_s during the peak growing season of maize in three counties in North China. A simple exponential model, which included the corresponding spatial proxies from remote sensing

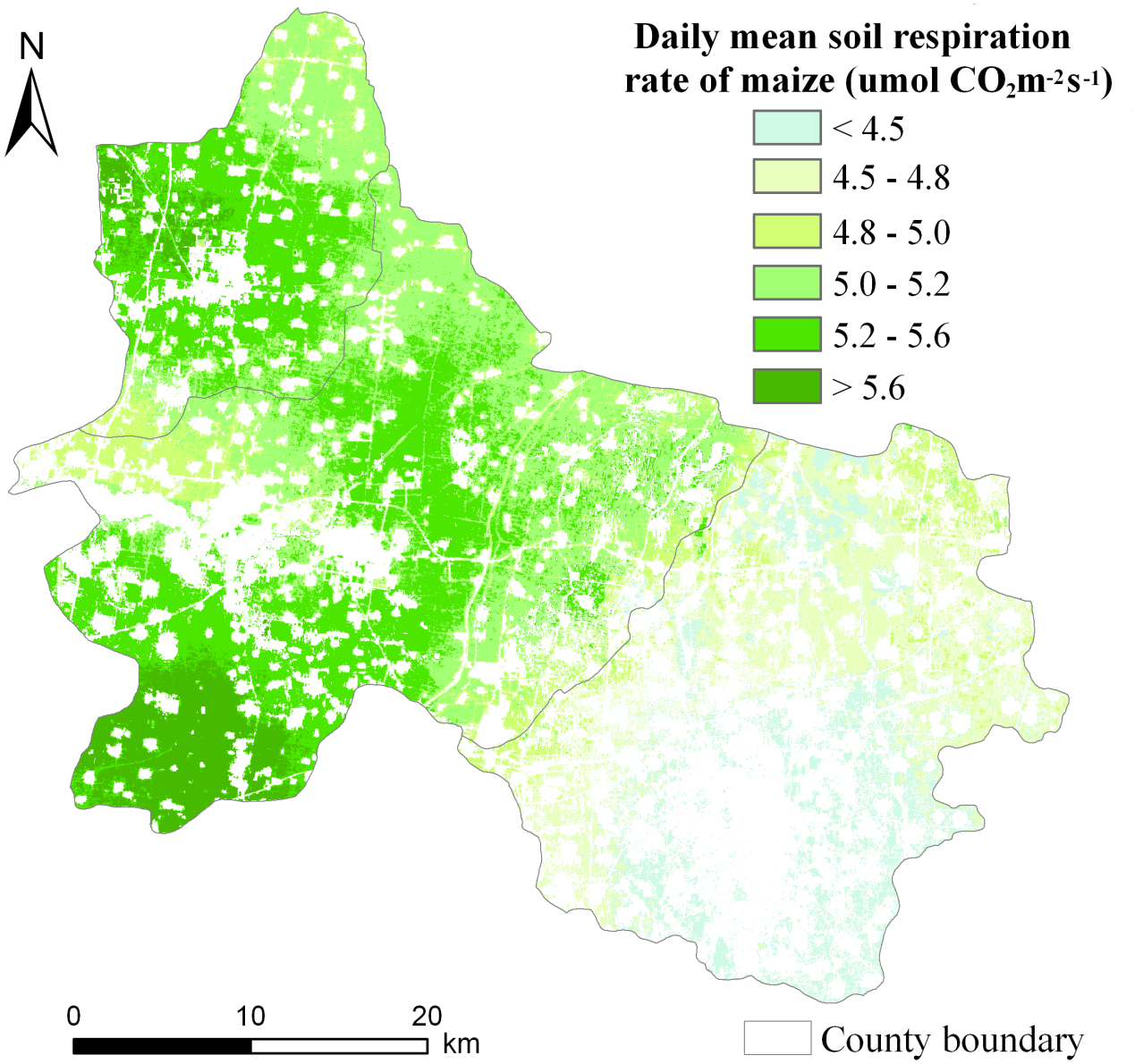

Figure 7. Spatial pattern of daily mean soil respiration rate during the peak growing season of maize in three counties in North China.
doi:10.1371/journal.pone.0105150.g007

and GIS (i.e., EVI and spatially interpolated SOC content), was employed. A similar method was applied to a deciduous broadleaf forest site in the Midwest USA [79]. The independent test data also demonstrated the rationality of this method at the study site to a certain extent (Fig. 8). Regardless of the form of the R_s model, the relationship between LAI and EVI, as well as the kriging interpolation precision of the SOC content, affected the predictive accuracy of the R_s model. A moderate correlation between EVI and LAI (Fig. 4) affected the test accuracy of the exponential model with an R^2 value of 0.69 and an RMSE value of 0.51 μmol CO_2 m^{-2} s^{-1} (Fig. 8). The tendency of kriging to overestimate small values is supported by previous studies [80–82]. This tendency may help explain the bias toward overestimating R_s at low values (Fig. 8). Therefore, improving the accuracy of input parameters from remote sensing or GIS will increase the predictive capability of the R_s model.

Notably, the R_s model developed in this study was applicable to maize fields during the peak growth period in the three counties in North China. However, the model employed in this study does not consider temperature, a main driver of R_s that has high spatial variability. This model may be not used anywhere else or in other stages of the growing season. Furthermore, when spatially distributed data were used in the R_s model, a simple alternative method was employed to estimate the maize LAI by using the remotely sensed EVI, which may be problematic. Verstraeten et al. [83] highlighted that the assimilation of remotely sensed geophysical products into a carbon model is a complex process, and simply exchanging conventional input data for their remotely sensed counterparts is insufficient. Therefore, future research should focus on an integrating spatially distributed R_s datasets and geophysical products from remote sensing and GIS by using the data assimilation method, which has been extensively applied in

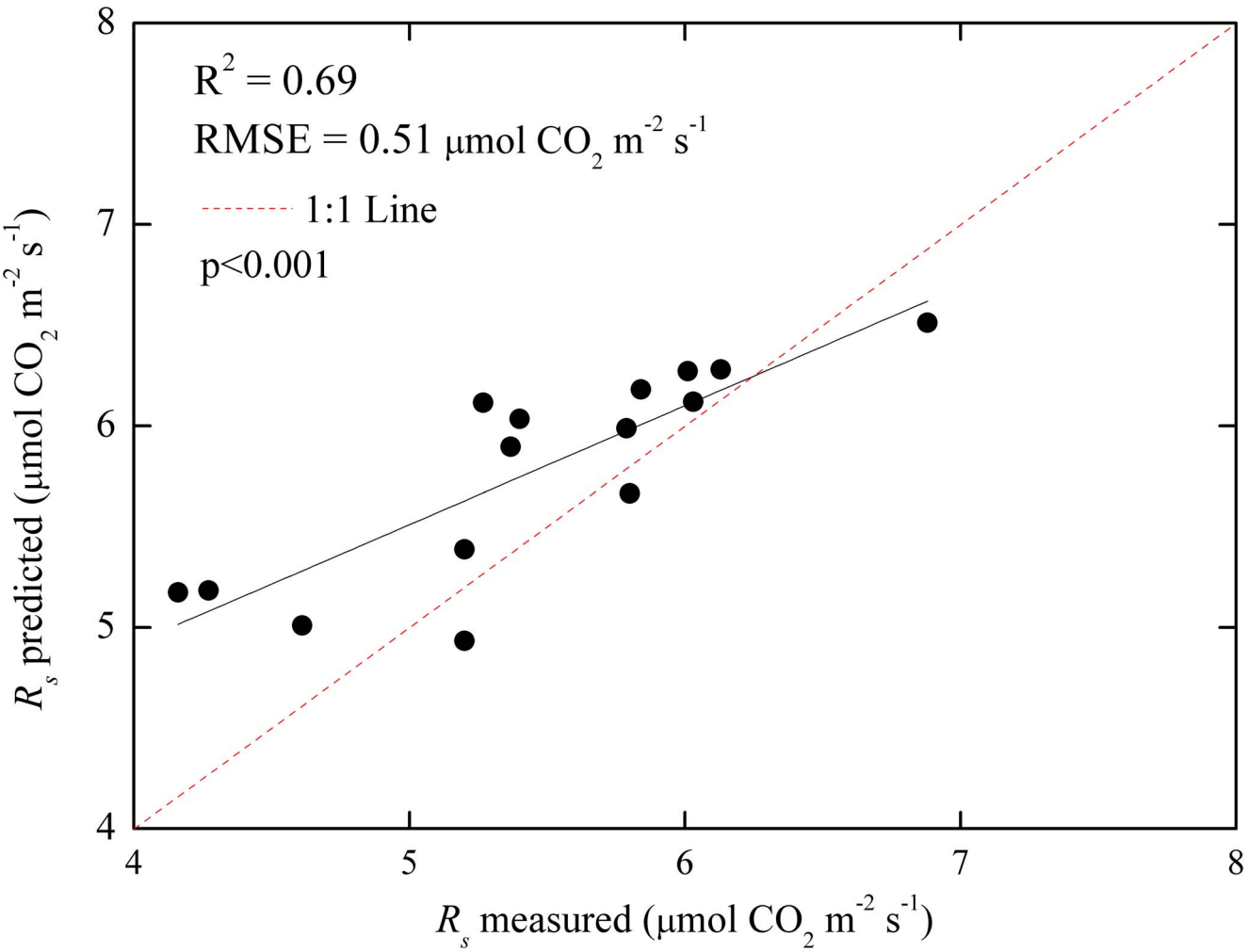

Figure 8. Spatial data predicted soil respiration (R_s) and corresponding ground-based measurements with R^2 and RMSE (μmol CO_2 m^{-2} s^{-1}) during the peak growing season of maize in three counties in North China (n = 15). The predicted soil respiration was attained with an exponential model that used EVI and SOC content as dependent variables.
doi:10.1371/journal.pone.0105150.g008

terrestrial carbon cycle research [84–86]. However, this method lack the integration of R_s and spatially distributed data.

Conclusions

This study investigated the potential of spatial data from remote sensing and GIS for estimating the spatial patterns of R_s during the peak growing season of maize in three counties in North China. Based on in situ measurements, plant productivity (i.e., LAI) and soil property (i.e. SOC content) factors were identified as the most important determinants of spatial variability in R_s during the peak growing season of maize, and R_s was weakly related to soil temperature and soil moisture. Spectral VIs calculated from an HJ-1A CCD optical image were used to estimate LAI and EVI was found to be the best proxy for LAI. To derive the spatial pattern of R_s during the peak growing season of maize, a simple exponential model, which included remotely sensed EVI and GIS spatially interpolated SOC content, was employed. This method was tested by using an independent sample dataset and was shown to be reasonable at the study site.

Acknowledgments

We sincerely thank the anonymous reviewers for their important and constructive revision advices on the manuscript.

Author Contributions

Conceived and designed the experiments: NH LW YQG. Performed the experiments: NH LW PYH. Analyzed the data: NH LW PYH. Contributed reagents/materials/analysis tools: NH LW YQG PYH ZN. Wrote the paper: NH.

References

1. Raich JW, Potter CS (1995) Global patterns of carbon dioxide emissions from soils. Global Biogeochemical Cycles 9: 23–36.
2. Davidson EA, Belk E, Boone RD (1998) Soil water content and temperature as independent or confound factors controlling soil respiration in a temperature mixed hardwood forest. Global Change Biology 4: 217–227.
3. Buchmann N (2000) Biotic and abiotic factors controlling soil respiration rates in Picea abies stands. Soil Biology and Biochemistry 32: 1625–1635.
4. Campbell JL, Sun OJ, Law BE (2004) Supply-side controls on soil respiration among Oregon forests. Global Change Biology 10: 1857–1869.

5. Webster KL, Creed IF, Skowronski MD, Kaheil YH (2009) Comparison of the performance of statistical models that predict soil respiration from forests. Soil Science Society of America Journal 73: 1157–1167.
6. Gaumont-Guay D, Black TA, Griffis TJ, Barr AG, Jassal RS, et al. (2006) Interpreting the dependence of soil respiration on soil temperature and water content in a boreal aspen stand. Agricultural and Forest Meteorology 140: 220–235.
7. Phillips SC, Varner RK, Frolking S, Munger JW, Bubier JL, et al. (2010). Interannual, seasonal, and diel variation in soil respiration relative to ecosystem respiration at a wetland to upland slope at Harvard Forest. Journal of Geophysical Research: Biogeosciences 115: G02019. doi: 10.1029/2008JG000858.
8. Reichstein M, Rey A, Freibauer A, Tenhunen J, Valentini R, et al. (2003) Modeling temporal and large-scale spatial variability of soil respiration from soil water availability, temperature and vegetation productivity indices. Global Biogeochemical Cycles 17: 1104. doi: 10.1029/2003GB002035.
9. Geng Y, Wang Y, Yang K, Wang S, Zeng H, et al. (2012) Soil respiration in Tibetan alpine grasslands: belowground biomass and soil moisture, but not soil temperature, best explain the large-scale patterns. PloS one 7: e34968. doi: 10.1371/journal.pone.0034968.
10. Huang N, Niu Z, Zhan YL, Tappertc MC, Wu CY, et al. (2012) Relationships between soil respiration and photosynthesis-related spectral vegetation indices in two cropland ecosystems. Agricultural and Forest Meteorology 160: 80–89.
11. Chen ST, Huang Y, Zou JW, Shen QR, Hu ZH, et al. (2010) Modeling interannual variability of global soil respiration from climate and soil properties. Agricultural and Forest Meteorology 150: 590–605.
12. Almagro M, Querejeta JI, Boix-Fayos C, Martínez-Mena M (2013) Links between vegetation patterns, soil C and N pools and respiration rate under three different land uses in a dry Mediterranean ecosystem. Journal of Soils and Sediments 13: 641–653.
13. Martin JG, Bolstad PV, Ryu SR, Chen J (2009) Modeling soil respiration based on carbon, nitrogen, and root mass across diverse Great Lake forests. Agricultural and Forest Meteorology 149: 1722–1729.
14. Longley P (Ed.) (2005) Geographic information systems and science. John Wiley & Sons.
15. Weng Q (2001) Modeling urban growth effects on surface runoff with the integration of remote sensing and GIS. Environmental Management 28: 737–748.
16. Lin ML, Chen CW (2011) Using GIS-based spatial geocomputation from remotely sensed data for drought risk-sensitive assessment. International Journal of Innovative Computing, Information and Control 7: 657–668.
17. Shalaby A, Tateishi R (2007) Remote sensing and GIS for mapping and monitoring land cover and land-use changes in the Northwestern coastal zone of Egypt. Applied Geography 27: 28–41.
18. Dewan AM, Yamaguchi Y (2009). Land use and land cover change in Greater Dhaka, Bangladesh: using remote sensing to promote sustainable urbanization. Applied Geography 29: 390–401.
19. Wang XD, Zhong XH, Liu SZ, Liu JG, Wang ZY, et al. (2008). Regional assessment of environmental vulnerability in the Tibetan Plateau: development and application of a new method. Journal of Arid environments 72: 1929–1939.
20. Ceccato P, Connor SJ, Jeanne I, Thomson MC (2005) Application of geographical information systems and remote sensing technologies for assessing and monitoring malaria risk. Parassitologia 47: 81–96.
21. Franklin J (1995) Predictive vegetation mapping: geographic modelling of biospatial patterns in relation to environmental gradients. Progress in Physical Geography 19: 474–499.
22. Raup B, Kääb A, Kargel JS, Bishop MP, Hamilton G, et al. (2007) Remote sensing and GIS technology in the Global Land Ice Measurements from Space (GLIMS) project. Computers & Geosciences 33: 104–125.
23. Keane RE, Burgan R, van Wagtendonk J (2001) Mapping wildland fuels for fire management across multiple scales: integrating remote sensing, GIS, and biophysical modeling. International Journal of Wildland Fire 10: 301–319.
24. He C, Wang S, Xu J, Zhou C (2002) Using remote sensing to estimate the change of carbon storage: a case study in the estuary of Yellow River delta. International Journal of Remote Sensing 23: 1565–1580.
25. Yuan W, Liu S, Yu G, Bonnefond JM, Chen J, et al. (2010) Global estimates of evapotranspiration and gross primary production based on MODIS and global meteorology data. Remote Sensing of Environment 114: 1416–1431.
26. Huang N, He JS, Niu Z (2013) Estimating the spatial pattern of soil respiration in Tibetan alpine grasslands using Landsat TM images and MODIS data. Ecological Indicators 26: 117–125.
27. Davidson EA, Richardson AD, Savage KE, Hollinger DY (2006) A distinct seasonal pattern of the ratio of soil respiration to total ecosystem respiration in a spruce-dominated forest. Global Change Biology 12, 230–239.
28. Vargas R, Baldocchi DD, Allen MF, Bahn M, Black TA, et al. (2010) Looking deeper into the soil: biophysical controls and seasonal lags of soil CO_2 production and efflux. Ecological Applications 20: 1569–1582.
29. Bondeau A, Smith PC, Zaehle S, Schaphoff S, Lucht W, et al. (2007) Modelling the role of agriculture for the 20th century global terrestrial carbon balance. Global Change Biology 13: 679–706.
30. Foley JA, DeFries RS, Asner GP, Barford C, Bonan G, et al. (2005) Global consequences of land use. Science 309: 570–574.
31. Krugh B, Bickham L, Miles D (1994) The solid-state chlorophyll meter: a novel instrument for rapidly and accurately determining the chlorophyll concentrations in seedling leaves. Maize Genetics Cooperation Newsletter 68: 25–27.
32. Wu CY, Wang L, Niu Z, Gao S, Wu MQ (2010) Nondestructive estimation of canopy chlorophyll content using Hyperion and Landsat/TM images. International Journal of Remote Sensing 31: 2159–2167.
33. Gao Y, Xie Y, Jiang H, Wu B, Niu J (2014) Soil water status and root distribution across the rooting zone in maize with plastic film mulching. Field Crops Research 156: 40–47.
34. Kou TJ, Zhu P, Huang S, Peng XX, Song ZW, et al. (2012) Effects of long-term cropping regimes on soil carbon sequestration and aggregate composition in rainfed farmland of Northeast China. Soil and Tillage Research 118: 132–138.
35. Nelson DW, Sommers LE (1982) Total carbon, organic carbon, and organic matter. In: Page AL, Miller RH, Keeney DR. (Eds.), Methods of Soil Analysis. American Society of Agronomy and Soil Science Society of American, Madison. 101–129.
36. Gallaher RN, Weldon CO, Boswell FC (1976) A semiautomated procedure for total nitrogen in plant and soil samples. Soil Science Society of America Journal 40: 887–889.
37. Wardlow BD, Egbert SL, Kastens JH (2007) Analysis of time-series MODIS 250 m vegetation index data for crop classification in the US Central Great Plains. Remote Sensing of Environment 108: 290–310.
38. Wilson EH, Sader SA (2002) Detection of forest harvest type using multiple dates of Landsat TM imagery. Remote Sensing of Environment 80: 385–396.
39. Zhong B, Ma P, Nie A, Yang A, Yao Y, et al. (2014) Land cover mapping using time series HJ-1/CCD data. Science China: Earth Sciences doi: 10.1007/s11430-014-4877-5.
40. Bian JH, Li AN, Jin HA, Lei GB, Huang CQ, et al. (2013) Auto-registration and orthorecification algorithm for the time series HJ-1A/B CCD images. Journal of Mountain Science 10: 754–767.
41. Liu Y, Li M, Mao L, Cheng L, Chen K (2013) Seasonal pattern of tidal-flat topography along the Jiangsu middle coast, China, using HJ-1 optical images. Wetlands 33: 871–886.
42. Wang SD, Miao LL, Peng GX (2012) An Improved Algorithm for Forest Fire Detection Using HJ Data. Procedia Environmental Sciences 13: 140–150.
43. Gamon JA, Field CB, Goulden ML, Griffin KL, Hartley AE, et al. (1995) Relationship between NDVI, canopy structure and photosynthesis in three Californian vegetation types. Ecological Applications 5: 28–41.
44. Hansen PM, Schjoerring JK (2003) Reflectance measurement of canopy biomass and nitrogen status in wheat crops using normalized difference vegetation indices and partial least squares regression. Remote Sensing of Environment 86: 542–553.
45. Yu X, Yan Q, Liu Z (2010) Atmospheric correction of HJ-1A multi-spectral and hyper-spectral images. Image and Signal Processing (CISP), 2010 3rd International Congress on. IEEE 5: 2125–2129.
46. Li P, Jiang L, Feng Z (2013) Cross-Comparison of Vegetation Indices Derived from Landsat-7 Enhanced Thematic Mapper Plus (ETM+) and Landsat-8 Operational Land Imager (OLI) Sensors. Remote Sensing 6: 310–329.
47. Rouse JW, Haas RH, Schell JA, Deering DW, Harlan JC (1974) Monitoring the vernal advancements and retrogradation of natural vegetation, In: NASA/GSFC, Final Report, Greenbelt, MD, USA, 1–137.
48. Gamon JA, Field CB, Goulden ML, Griffin KL, Hartley AE, et al. (1995) Relationship between NDVI, canopy structure and photosynthesis in three Californian vegetation types. Ecological Applications 5: 28–41.
49. Qi J, Chehbouni A, Huete AR, Kerr YH, Sorooshian S (1994) A modified soil adjusted vegetation index (MSAVI). Remote Sensing of Environment 48: 119–126.
50. Huete A, Didan K, Miura T, Rodriguez EP, Gao X, et al. (2002) Overview of the radiometric and biophysical performance of the MODIS vegetation indices. Remote Sensing of Environment 83: 195–213.
51. Broge NH, Leblanc E (2001) Comparing prediction power and stability of broadband and hyperspectral vegetation indices for estimation of green leaf area index and canopy chlorophyll density. Remote Sensing of Environment 76: 156–172.
52. Haboudane D, Miller JR, Tremblay N, Zarco-Tejada PJ, Dextraze L (2002) Integrated narrow-band vegetation indices for prediction of crop chlorophyll content for application to precision agriculture. Remote Sensing of Environment 81: 416–426.
53. Gitelson AA, Vina A, Ciganda V, Rundquist DC, Arkebauer TJ (2005) Remote estimation of canopy chlorophyll content in crops. Geophysical Research Letters 32: L08403. doi: 10.1029/2005GL022688.
54. Wu C, Niu Z, Tang Q, Huang W (2008) Estimating chlorophyll content from hyperspectral vegetation indices: Modeling and validation. Agricultural and Forest Meteorology 148: 1230–1241.
55. Hirose T, Ackerly DD, Traw MB, Ramseier D, Bazzaz FA (1997) CO_2 elevation, canopy photosynthesis, and optimal leaf area index. Ecology 78: 2339–2350.
56. Gitelson AA, Vina A, Verma SB, Rundquist DC, Arkebauer TJ, et al. (2006) Relationship between gross primary production and chlorophyll content in crops: Implications for the synoptic monitoring of vegetation productivity. Journal of Geophysical Research-Atmospheres 111: D08S11. doi: 10.1029/2005JD006017.
57. Glenn EP, Huete AR, Nagler PL, Nelson SG (2008) Relationship between remotely-sensed vegetation indices, canopy attributes and plant physiological

processes: what vegetation indices can and cannot tell us about the landscape. Sensors 8: 2136–2160.
58. Huang N, Niu Z (2013) Estimating soil respiration using spectral vegetation indices and abiotic factors in irrigated and rainfed agroecosystems. Plant and Soil 367: 535–550.
59. Chevallier T, Voltz M, Blanchart E, Chotte JL, Eschenbrenner V, et al. (2000) Spatial and temporal changes of soil C after establishment of a pasture on a long-term cultivated vertisol (Martinique). Geoderma 94: 43–58.
60. McGrath D, Zhang C (2003) Spatial distribution of soil organic carbon concentrations in grassland of Ireland. Applied Geochemistry 18: 1629–1639.
61. Liu D, Wang Z, Zhang B, Song K, Li X, et al. (2006) Spatial distribution of soil organic carbon and analysis of related factors in croplands of the black soil region, Northeast China. Agriculture, Ecosystems & Environment 113: 73–81.
62. Matheron G (1963) Principles of geostatistics. Economic geology 58: 1246–1266.
63. Webster R, Oliver MA (2007) Geostatistics for environmental scientists. John Wiley & Sons.
64. Raich JW, Tufekciogul A (2000) Vegetation and soil respiration: correlations and controls. Biogeochemistry 48: 71–90.
65. Schaefer DA, Feng W, Zou X (2009) Plant carbon inputs and environmental factors strongly affect soil respiration in a subtropical forest of southwestern China. Soil Biology and Biochemistry 41: 1000–1007.
66. Curiel Yuste J, Baldocchi DD, Gershenson A, Goldstein A, Misson L, et al. (2007) Microbial soil respiration and its dependency on carbon inputs, soil temperature and moisture. Global Change Biology 13: 2018–2035.
67. Pugesek BH, Tomer A, Von Eye A (Eds.) (2003) Structural equation modeling: applications in ecological and evolutionary biology. Cambridge University Press.
68. Iriondo JM, Albert MJ, Escudero A (2003) Structural equation modelling: an alternative for assessing causal relationships in threatened plant populations. Biological Conservation 113: 367–377.
69. Jonsson M, Wardle DA (2010) Structural equation modelling reveals plant-community drivers of carbon storage in boreal forest ecosystems. Biology Letters 6: 116–119.
70. Kim GS (2010) AMOS 18.0: Structural Equation Modeling. Seoul: Hannarae Publishing Co.
71. National Bureau of statistics of China (2006) China social-economic statistical yearbooks for China's counties and cities. China Statistics Press, Beijing.
72. Wang S, Tian H, Liu J, Pan S (2003) Pattern and change of soil organic carbon storage in China: 1960s–1980s. Tellus B 55: 416–427.
73. West TO, Post WM (2002) Soil organic carbon sequestration rates by tillage and crop rotation. Soil Science Society of America Journal 66: 1930–1946.
74. Wilhelm WW, Johnson JM, Karlen DL, Lightle DT (2007) Corn stover to sustain soil organic carbon further constrains biomass supply. Agronomy journal 99: 1665–1667.
75. Foley JA (1995) An equilibrium model of the terrestrial carbon budget. Tellus B 47: 310–319.
76. Lal R (1999) Soil management and restoration for C sequestration to mitigate the accelerated greenhouse effect. Progress in Environmental Science 1: 307–326.
77. Epron D, Bosc A, Bonal D, Freycon V (2006) Spatial variation of soil respiration across a topographic gradient in a tropical rain forest in French Guiana. Journal of Tropical Ecology 22: 565–574.
78. Suyker AE, Verma SB, Burba GG, Arkebauer TJ (2005) Gross primary production and ecosystem respiration of irrigated maize and irrigated soybean during a growing season. Agricultural and Forest Meteorology 131: 180–190.
79. Huang N, Gu L, Niu Z (2014) Estimating soil respiration using spatial data products: A case study in a deciduous broadleaf forest in the Midwest USA. Journal of Geophysical Research: Atmospheres 119. doi:10.1002/2013JD020515.
80. Hudak AT, Lefsky MA, Cohen WB, Berterretche M (2002) Integration of lidar and Landsat ETM+ data for estimating and mapping forest canopy height. Remote Sensing of Environment 82: 397–416.
81. Meng Q, Cieszewski C, Madden M (2009) Large area forest inventory using Landsat ETM+: a geostatistical approach. ISPRS Journal of Photogrammetry and Remote Sensing 64: 27–36.
82. Tsui OW, Coops NC, Wulder MA, Marshall PL (2013) Integrating airborne LiDAR and space-borne radar via multivariate kriging to estimate above-ground biomass. Remote Sensing of Environment 139: 340–352.
83. Verstraeten WW, Veroustraete F, Wagner W, Van Roey T, Heyns W, et al. (2010) Remotely sensed soil moisture integration in an ecosystem carbon flux model-The spatial implication. Climatic Change 103:117–136.
84. Rayner PJ, Scholze M, Knorr W, Kaminski T, Giering R, et al. (2005) Two decades of terrestrial carbon fluxes from a carbon cycle data assimilation system (CCDAS). Global Biogeochemical Cycles 19.
85. Chevallier F, Bréon FM, Rayner PJ (2007) Contribution of the Orbiting Carbon Observatory to the estimation of CO_2 sources and sinks: Theoretical study in a variational data assimilation framework. Journal of Geophysical Research: Atmospheres 112: D09307. doi: 10.1029/2006JD007375.
86. Knorr W, Kaminski T, Scholze M, Gobron N, Pinty B, et al. (2010) Carbon cycle data assimilation with a generic phenology model. Journal of Geophysical Research: Biogeosciences 115: G04017. doi: 10.1029/2009JG001119.